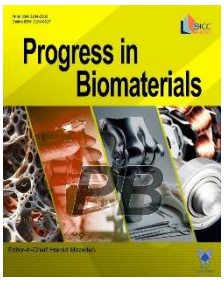


Volume 15, Issue 4, 2025: Article 19

Progress in Biomaterials (PIBM)

https://doi.org/10.57647/pibm-2025-17326

# Biogenically Synthesized Zinc Oxide Nanoparticles using *Penicillium chrysogenum* Filter to Combat Methicillin-resistant *Staphylococcus aureus* (MRSA) and Cancer Cells

Mohamed A. Fareid [1], Gamal M. El-Sherbiny*[2], Mohamed H. Sharaf [2], Ahmed A. Radwan [2], Asmaa M. Hegazy [1], Rosilah Ab Aziz [3], Fatma A. Hamada [3]

[1]*Clinical Laboratory Science Department, Applied Medical Science College, University of Ha'il, Hail 2440, Saudi Arabia*
[2]*Botany and Microbiology Department, Faculty of Science, Al-Azhar University, Cairo 11884, Egypt*
[3]*First Year of Health and Medical Colleges, Basic Sciences Department, University of Ha'il, Hail 2440, Saudi Arabia*

***Corresponding author:** gamalelsherbiny1970@yahoo.com

**Original Research**

Received:
14 September 2025

Accepted:
28 October 2025

Published in Issue:
30 December 2025



**Abstract**

*Staphylococcus aureus* is a major opportunistic pathogen that persistently colonizes approximately 20% of the human population. It is capable of causing diverse infections ranging from mild skin lesions to severe, life-threatening conditions. The emergence of methicillin-resistant *S. aureus* (MRSA) has complicated treatment strategies and intensified the search for alternative antimicrobial agents. This study presents a novel, eco-friendly biosynthesis of zinc oxide nanoparticles (ZnO-NPs) using the cell-free filtrate of *Penicillium chrysogenum* and investigates their antibacterial, anti-virulence, antioxidant, and anticancer activities. The synthesized ZnO-NPs were characterized using UV-Visible spectroscopy, high-resolution transmission electron microscopy (HR-TEM), dynamic light scattering (DLS), zeta potential and X-ray diffraction (XRD). Antibacterial efficacy was determined against MRSA isolates through MIC assays, while biofilm inhibition and virulence gene expression analyses were performed to assess anti-virulence activity. Antioxidant capacity was evaluated using DPPH and ABTS assays, and cytotoxicity against HepG2 and MCF-7 cancer cell lines was assessed using MTT assays. UV-Vis spectra exhibited a distinct absorption peak at 430 nm. HR-TEM analysis revealed predominantly spherical to slightly irregular ZnO-NPs with an average diameter of 43.17 nm (ranging 50-70.25 nm). The biosynthesized ZnO-NPs demonstrated strong antibacterial activity against MRSA, with MIC values between 125 and 250 µg/mL, and significantly inhibited biofilm formation. Moreover, they downregulated key virulence genes by 2.0 - 4.6-fold. The nanoparticles also exhibited notable antioxidant activity with $IC_{50}$ values of 205 µg/mL (DPPH) and 315 µg/mL (ABTS), as well as potent anticancer effects with $IC_{50}$ values of 13.74 ± 0.02 µg/mL (HepG2) and 19.12 ± 0.51 µg/mL (MCF-7). This study demonstrates, for the first time, the biosynthesis of ZnO-NPs using *P. chrysogenum* filtrate with multi-functional bioactivity, including antibacterial, anti-virulence, antioxidant, and anticancer properties. These findings highlight the potential application of biosynthesized ZnO-NPs as promising biocompatible agents

for combating MRSA infections and certain cancer types, paving the way for sustainable nanotherapeutic development.

**Keywords:** *Staphylococcus aureus*; MRSA; *Penicillium chrysogenum*; Zinc oxide nanoparticles; Biosynthesis; Antibacterial; Antioxidant; Anticancer

**Cite this article:** Fareid M.A., El-Sherbiny G.M., Sharaf M.H., Radwan A.A., Hegazy A.M., Aziz R.A., Hamada F.A., Biogenically synthesized zinc oxide nanoparticles using *Penicillium chrysogenum* filter to combat methicillin-resistant *Staphylococcus aureus* (MRSA) and Cancer Cells. *Progress in Biomaterials 15(4), Article 19.* https://doi.org/10.57647/pibm-2025-17326

## Graphical abstract

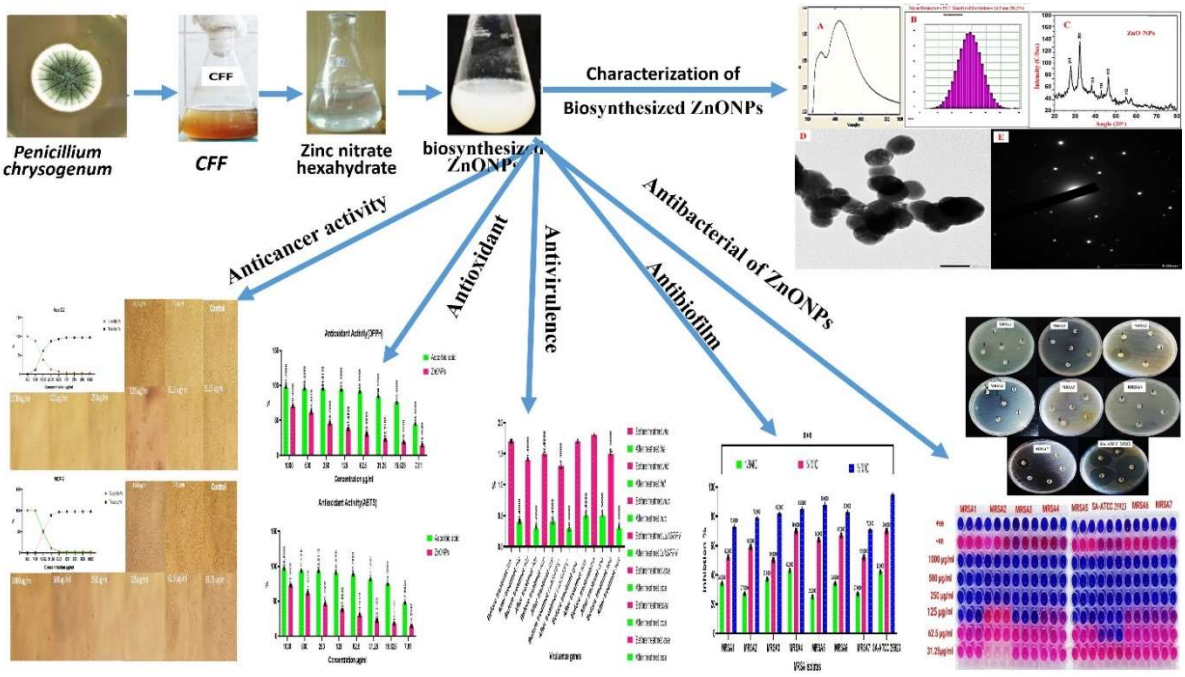


## 1. Introduction

*Staphylococcus aureus* is a well-recognized opportunistic pathogen responsible for a wide range of infections, from minor skin conditions to severe diseases such as endocarditis and osteoarticular infections, both of which are associated with high morbidity and mortality. Methicillin-resistant *Staphylococcus aureus* (MRSA) poses a particularly serious and unpredictable threat due to its remarkable adaptability and resistance to multiple antibiotic classes. Its exceptional genetic plasticity and the continual emergence of epidemic strains have made it a persistent global public health concern. Moreover, the extracellular polymeric matrix of *S. aureus* biofilms facilitates the development of multidrug-resistant populations and hinders antibiotic penetration, further complicating treatment [1].

The pathogenicity of *S. aureus* is mediated by a diverse array of virulence factors encoded by specific genes. Among them, alpha-hemolysin-encoded by *hla*-is an exotoxin associated with severe skin and soft tissue infections, while delta-hemolysin, encoded by *hld*, disrupts host cell membranes [2]. Another major virulence determinant is Panton-Valentine leukocidin (PVL), encoded by *LukS/F-PV*, which targets leukocytes and induces tissue necrosis. Additional important virulence genes include *spa* (Staphylococcal protein A), *coa* (coagulase), and *sea* (Staphylococcal enterotoxin A), all of which contribute to immune evasion and pathogenesis. The *spa* gene product inhibits phagocytosis, allowing bacterial persistence, while coagulase-encoded by *coa*-induces blood clotting, forming a fibrin barrier around the bacteria. The *sea* gene encodes enterotoxin A, responsible for staphylococcal food poisoning [3].

The rapid rise of multidrug-resistant pathogens has intensified the search for novel and effective alternatives to conventional antibiotics. Developing such alternatives

not only addresses the antimicrobial resistance crisis but also offers cost-effective and sustainable strategies compared with traditional antibiotic discovery, which is labor-intensive and time-consuming. In this regard, nanostructure-derived antimicrobials represent a promising approach to overcoming bacterial resistance mechanisms [1].

Nanotechnology, defined as the manipulation of materials at the atomic or molecular level, has emerged as a highly interdisciplinary and dynamic field integrating engineering, chemistry, and biology. Nanoparticles (NPs), typically less than 100 nm in size, exhibit unique physical, optical, and chemical properties that differ from their bulk counterparts [4]. Two principal approaches are employed in nanoparticle synthesis: top-down and bottom-up. Physical and chemical methods can efficiently produce nanoparticles but often require hazardous reagents, stabilizers, and high energy inputs, making them environmentally unsustainable and difficult to scale [5]. In contrast, biological (bio-fabricated) synthesis offers a safer, eco-friendly, and cost-effective alternative by utilizing natural reducing and capping agents derived from microorganisms and plants [5,6].

Various biological systems-including bacteria, actinobacteria, fungi, algae, cyanobacteria, and higher plants-have been successfully employed to biosynthesize metal-based nanoparticles [4]. Among these, fungi stand out as ideal biofactories due to their ease of cultivation, high biomass yield, tolerance to metal stress, and secretion of extracellular enzymes and metabolites that facilitate nanoparticle formation [7,8]. These metabolites-such as proteins, terpenoids, phenolics, flavonoids, and polysaccharides-act as natural reducing and stabilizing agents, influencing the nanoparticles' size, morphology, and surface charge. For example, nitrate reductase enzymes promote the reduction of metal ions, while phenolic and flavonoid compounds cap the nanoparticles, enhancing their stability and uniformity [9-13].

Zinc oxide nanoparticles have attracted substantial attention due to their unique physicochemical and biological properties. Zinc, an essential trace element, plays critical roles in DNA replication, repair, oxidative stress regulation, and cell cycle progression. ZnO-NPs are particularly valued for their low toxicity, high biocompatibility, strong antibacterial activity, antioxidant potential, and adjustable optical and photocatalytic characteristics [4,10,11]. Their nanoscale size enhances interactions with cellular membranes, nucleic acids, and receptors, making them valuable in a variety of biomedical applications, including bioimaging, diabetes therapy, drug delivery, antibacterial and anti-inflammatory treatments, wound healing, and anticancer therapy [12-,15].

Among biological systems, fungi offer exceptional potential for the biosynthesis of ZnO-NPs. They produce abundant extracellular enzymes and secondary metabolites that act as natural capping and reducing agents, leading to the synthesis of stable nanoparticles with desirable biofunctional properties [16-19]. Recent studies have shown that myco-synthesized ZnO-NPs from *Aspergillus niger*, *Trichoderma viride*, *Cochliobolus geniculatus*, *Alternaria tenuissima*, and *Penicillium chrysogenum* exhibit strong antibacterial, antioxidant, and anticancer activities [12,20-22]. *Penicillium chrysogenum* is particularly advantageous for nanoparticle biosynthesis due to its robust growth rate, secretion of extracellular enzymes, and industrial importance as a producer of penicillin. Its cell-free filtrate contains abundant biomolecules-such as proteins, organic acids, and phenolics-that effectively mediate metal ion reduction and nanoparticle stabilization [12,20-22].

Additionally, ZnO-NPs are also recognized as safe materials by the U.S. Food and Drug Administration (FDA) and are widely used due to their stability, biocompatibility, and low toxicity at physiologically relevant concentrations [11]. Myco-synthesized ZnO-NPs have demonstrated inhibitory activity against a broad range of bacteria, including Gram-positive (*S. aureus*, *S. epidermidis*, *B. subtilis*, *E. faecalis*) and Gram-negative species (*E. coli*, *P. aeruginosa*, *K. pneumoniae*, *P. mirabilis*) at concentrations of 25-100 µg/mL [9]. Furthermore, ZnO-NPs exert anticancer effects through mechanisms involving necrosis, apoptosis, and autophagy, with reported cytotoxicity against breast, lung, and prostate cancer cells [23]. Studies also suggest that Gram-positive bacteria are more susceptible to ZnO-NPs than Gram-negative bacteria, likely due to structural differences in cell wall composition and membrane permeability [24]. Vinotha et al. [25], developed ZnO nanocomposites incorporating *Acorus calamus* extract and a bacterial toxin protein (Cry), which showed concentration-dependent inhibition of *S. aureus* (MTCC 9542) biofilms [26]. Another study reported that ZnO nanocomposites loaded with pancreatin exhibited reduced cytotoxicity to human cells and enhanced anti-biofilm, anti-motility, and antibiotic-sensitizing effects against MRSA [27].

The novelty of this study lies in being the first to report the biosynthesis of ZnO-NPs using the cell-free filtrate of *Penicillium chrysogenum* and to comprehensively evaluate their antibacterial, anti-virulence, antioxidant, and anticancer activities.

This research establishes an environmentally sustainable and biologically driven approach for ZnO-NP synthesis, presenting a promising alternative to conventional chemical methods. The biosynthesized ZnO-NPs exhibited remarkable efficacy against methicillin-resistant *Staphylococcus aureus*, effectively reduced virulence factors, and showed potent antioxidant and anticancer properties-highlighting their potential as multifunctional, eco-friendly nanotherapeutic agents.

## 2. Materials and Methods

### 2.1. Chemicals

Zinc nitrate hexahydrate ($Zn(NO_3)_2 \cdot 6H_2O$, 99.99%) and ethylenediamine (EDA, $C_2H_4(NH_2)_2$, ≥99%) were supplied by Sigma–Aldrich (USA). Pure SiC nanowires (99%) were obtained from Changsha Sinet Advanced Materials (China). Sodium hydroxide (NaOH) and anhydrous ethanol were purchased from Acros Co. (Belgium). All solvents were of analytical grade and used without further purification.

### 2.2. Microorganisms

MRSA strains previously isolated and identified [1], along with *Staphylococcus aureus* ATCC 25923 and *Penicillium chrysogenum* ATCC-10106, were obtained from the Bacteriology Laboratory, Botany and Microbiology Department, Faculty of Science, Al-Azhar University, Cairo, Egypt.

### 2.3. Preparation of cell free filter of *Penicillium chrysogenum*

A fungal strain was inoculated into a 250 mL Erlenmeyer flask containing 50 mL of yeast extract liquid medium. Inoculation was performed using a 0.4 cm diameter mycelial disk obtained from seven-day-old culture plates of the test isolate. The cultures were incubated on a rotary shaker at 200 rpm and 30 °C, with an initial pH of 6.5, for four days. After incubation, the fungal biomass was separated from the culture broth by filtration through a 0.44 µm PVDF filter, followed by centrifugation at 10,000 rpm to remove any remaining cells and macromolecules [4, 28].

2.3.1. *Extracellular fabrication of ZnO-NPs by Penicillium chrysogenum* filter

A 1 mM aqueous solution of zinc nitrate hexahydrate (50 mL) was mixed with 50 mL of the cell-free filtrate (CFF) of *Penicillium chrysogenum*, and the pH of the mixture was adjusted to 8.5. The reaction mixture was incubated in a rotary shaker at 37 °C and 200 rpm in the dark for 24 hours. Control experiments using uninoculated medium and zinc nitrate solution were performed to assess the specific role of the fungal filtrate in nanoparticle synthesis. The reduction of zinc ions was monitored by collecting approximately 2 mL of the reaction mixture at various time intervals and analyzing it using a UV–Vis spectrophotometer (JASCO V-560). A visible color change and the appearance of a white suspension in each reaction vessel indicated the formation of ZnO nanoparticles. The resulting ZnO nanoparticle suspension was centrifuged at 12,000 rpm for 30 minutes, and the obtained pellets were dried in a hot-air oven at 60 °C until a constant weight was achieved [4, 28].

2.3.2. *Characterization of Biosynthesized ZnO-NPs*

The biosynthesized ZnO nanoparticles were characterized using various analytical techniques. UV–Visible spectroscopy was performed with a JASCO V-560 spectrophotometer (Tokyo, Japan) over a wavelength range of 200–900 nm with a resolution of 1 nm. For dynamic light scattering (DLS) analysis, the nanoparticle suspension was diluted tenfold with deionized water prior to measurement. Morphological and size analyses were carried out using High-Resolution Transmission Electron Microscopy (HR-TEM) on a JEOL JEM-100 CX instrument (Peabody, USA). For TEM observation, a drop of the ZnO nanoparticle suspension was placed on carbon-coated copper grids and air-dried. Prior to X-ray diffraction (XRD) analysis, the samples were centrifuged, and the resulting precipitate was dried under vacuum. XRD patterns were recorded using a Shimadzu XRD-6000 diffractometer (Tokyo, Japan). Dynamic light scattering (DLS) and zeta potential measurements were performed using a Malvern Zetasizer at the National Center for Radiation Research and Technology (NCRRT), Cairo, Egypt, within a measurement range of 0.1–1000 nm [1,4].

### 2.4. Antibacterial activity of biosynthesized ZnONPs

Antibacterial activity was assessed using the disc diffusion method against MRSA and *Staphylococcus aureus* ATCC 25923. Mueller-Hinton agar plates were prepared and inoculated with bacterial cultures adjusted to a 0.5 McFarland standard. Sterile discs were impregnated with 100 µL of the ZnO nanoparticle solution (5 mg), while standard antibiotic discs containing cefoxitin (10 µg), ampicillin (10 µg), erythromycin (15 µg), and gentamicin (10 µg) (Oxoid, England) served as positive controls. The plates were

initially stored at 4 °C for 2 hours to facilitate diffusion and subsequently incubated at 37 °C for 24 hours. Antibacterial activity was determined by measuring the diameter of the inhibition zones around each disc[1].

### 2.5. MIC of biosynthesized ZnO-NPs

The minimum inhibitory concentration (MIC) of ZnO nanoparticles against MRSA strains and *Staphylococcus aureus* ATCC 25923 was determined using the broth microdilution method. A sterile 96-well microtiter plate was prepared by dispensing 100 µL of double-strength Mueller-Hinton broth (MHB) (HiMedia, India) into each well, followed by serial dilutions to obtain final ZnO-NP concentrations of 1000, 500, 250, 125, 62.5, 31.25, 15.75, and 7.8 µg/mL. A 5% (v/v) bacterial suspension, adjusted to a 0.5 McFarland standard, was added to each well except the controls. Two controls were included: one containing MHB and the bacterial suspension to verify bacterial growth (positive control), and another containing MHB and ZnO-NPs without bacteria to ensure sterility (negative control). After incubation at 37 °C for 24 hours, 30 µL of 0.18% (w/v) resazurin solution (HiMedia) was added to each well to assess bacterial viability, followed by an additional 4-hour incubation. A color change from blue to pink, purple, or red indicated bacterial growth, while wells that remained blue signified inhibition. The experiment was conducted in triplicate, and the average MIC values were recorded [29,30].

### 2.6. Antibiofilm activity of biosynthesized ZnO-NPs

The antibiofilm activity of the biosynthesized ZnO nanoparticles was evaluated using sterile, flat-bottomed polystyrene 96-well microtiter plates, following the method described by Fareid *et al.* [1] with minor modifications. Briefly, each well was filled with 100 µL of Mueller-Hinton broth (MHB) and inoculated with 10 µL of an overnight culture of MRSA isolates or the reference strain *Staphylococcus aureus* ATCC 25923, adjusted to an optical density ($OD_{620}$) of 0.05 ± 0.02. Subsequently, 100 µL of ZnO nanoparticle suspensions at concentrations corresponding to ½ MIC, ¼ MIC, and ⅛ MIC were added to the wells. The plates were incubated at 37 °C for 48 hours. After incubation, the biofilms were fixed with absolute ethanol and stained with 0.1% (w/v) crystal violet for 30 minutes. The wells were then washed, air-dried, and treated with 200 µL of 33% acetic acid to solubilize the bound dye. The optical density (OD) of the solubilized crystal violet was measured at 630 nm using a microplate reader. The percentage of biofilm inhibition was calculated using the following formula:

Biofilm inhibition (%) = [(OD control − OD treated) / OD control] × 100

### 2.7. Effect of ZnO-NPs on expression level of virulence genes

MRSA isolates were cultured in tubes containing 6 mL of Tryptone Soya Broth (Sigma-Aldrich, St. Louis, MO, USA) supplemented with ½ MIC of ZnO nanoparticles (ZnO-NPs). Control tubes containing MRSA isolates without ZnO-NPs were included. All cultures were incubated at 37 °C for 24 hours. After incubation, the bacterial suspensions were transferred to sterile microcentrifuge tubes and centrifuged at 15,000 × *g* for 15 minutes. The supernatant was discarded, and the resulting pellet was resuspended in 200 µL of molecular-grade, nuclease-free water, followed by a second centrifugation at 15,000 × *g* for 10 minutes. The final pellet was reconstituted in 100 µL of TE buffer for RNA extraction. Total bacterial RNA was extracted from *S. aureus* isolates using the Easy-Spin™ Total RNA Extraction Kit (iNtRON Biotechnology, South Korea) with the addition of lysozyme (10 mg/mL), according to the manufacturer's instructions. The expression levels of selected virulence genes (*nuc*, *lukS/F-PV*, *hla*, *hld*, *spa*, *coa*, *sea*, and *16S rRNA*) were quantified using quantitative reverse transcription PCR (qRT-PCR). The *16S rRNA* gene served as the internal reference. qRT-PCR reactions were performed using the SensiFAST SYBR Lo-ROX One-Step Kit (Meridian Life Science, UK) following the manufacturer's protocol. Each 20 µL reaction mixture contained 10 µL of master mix, 0.8 µL each of forward and reverse primers, 0.2 µL of reverse transcriptase, 0.4 µL of RNase inhibitor, 4 µL of template RNA, and nuclease-free water to a final volume of 20 µL. Negative controls (with deionized water instead of template RNA) were included in each run. Thermal cycling conditions were as follows: reverse transcription at 45 °C for 10 minutes, polymerase activation at 95 °C for 2 minutes, followed by 40 cycles of denaturation at 95 °C for 5 seconds and annealing/extension at 60 °C for 20 seconds. PCR products were analyzed by gel electrophoresis to verify specificity and the absence of non-specific products. Relative gene expression levels were calculated using the $2^{-\Delta\Delta Ct}$ method [31,32].

### 2.8. Antioxidant activity

#### 2.8.1. *DPPH assay*

The antioxidant activity of ZnO nanoparticles (ZnO-NPs) and ascorbic acid was evaluated across a concentration range of 7.81–1000 µg/mL using the

DPPH (2,2-diphenyl-1-picrylhydrazyl) assay. To assess free radical scavenging activity, 100 µL of DPPH solution was mixed with 100 µL of the test sample in a 96-well microplate and incubated at 25 °C for 30 minutes in the dark. After incubation, the absorbance was measured at 490 nm using a microplate reader, with pure methanol (100%) serving as the blank control. The percentage of DPPH radical scavenging activity was calculated using the following formula:

$$\text{DPPH scavenging activity (\%)} = \frac{A_{\text{control}} - A_{\text{sample}}}{A_{\text{control}}} \times 100$$

where $A_{\text{control}}$ is the absorbance of the control (DPPH solution without sample) and $A_{\text{sample}}$ is the absorbance in the presence of ZnO-NPs or ascorbic acid.

The antioxidant efficacy of ZnO-NPs and ascorbic acid was further compared based on their $IC_{50}$ values, defined as the concentration required to scavenge 50% of the DPPH radicals [34].

2.8.2. *ABTS assay*

The antioxidant capacity of ZnO nanoparticles (ZnO-NPs) was further evaluated using the ABTS (2,2′-azino-bis(3-ethylbenzothiazoline-6-sulfonic acid)) assay, following the method described by El-Sherbiny et al. [34]. The ABTS radical scavenging activity (%) was calculated using the following equation:

$$\text{ABTS scavenging activity (\%)} = \frac{A_{\text{control}} - A_{\text{sample}}}{A_{\text{control}}} \times 100$$

where $A_{\text{control}}$ is the absorbance of the ABTS radical solution without the sample, and $A_{\text{sample}}$ is the absorbance in the presence of ZnO-NPs.

### 2.9. Cytotoxicity study

An *in vitro* cytotoxicity assessment of ZnO nanoparticles (ZnO-NPs) was performed using the MTT assay, following the method described by El-Sherbiny et al. [35]. The human breast cancer (MCF-7) and liver carcinoma (HepG2) cell lines were obtained from the American Type Culture Collection (ATCC, Rockville, USA). The cells were exposed to various concentrations of ZnO-NPs ranging from 31.25 to 1000 µg/mL and incubated at 37 °C for 24 hours. After incubation, the culture medium was removed, and the cells were washed three times with either fresh medium or cold phosphate-buffered saline (PBS). Subsequently, the cells were treated with MTT solution (0.5 mg/mL) for 2–5 hours to allow the formation of formazan crystals. The MTT solution was then discarded, and 200 µL of dimethyl sulfoxide (DMSO) was added to each well to solubilize the formazan crystals. The optical density (OD) was measured at 570 nm using a microplate reader. Cell viability and cytotoxicity percentages were calculated using the following equations:

$$\text{Cell viability (\%)} = \left(\frac{\text{OD of treated cells}}{\text{OD of control cells}}\right) \times 100$$

$$\text{Cell death (\%)} = \left(\frac{\text{OD of control} - \text{OD of sample}}{\text{OD of control}}\right) \times 100$$

**Statistical analysis**

All results are expressed as the mean ± standard deviation (SD) from experiments performed in triplicate. Statistical comparisons between experimental and control groups were conducted using one-way and two-way analyses of variance (ANOVA), as appropriate. Data analyses were performed using GraphPad Prism software version 8.0 (GraphPad Software, Inc., La Jolla, CA, USA). Differences were considered statistically significant at $p < 0.05$.

## 3. Results and discussion

### 3.1. Extracellular bio-fabrication and Characterization of ZnO-NPs

The extracellular synthesis of ZnO nanoparticles was achieved by mixing a cell-free filtrate (CFF) of *Penicillium chrysogenum* with an equal volume of zinc nitrate hexahydrate precursor (1:1 v/v). The initial indication of successful ZnO-NP biosynthesis was a color change in the zinc nitrate solution from colorless to yellowish-white or turbid white upon the aseptic addition of the CFF. The use of fungal-derived CFF for metal nanoparticle synthesis has been well documented in prior studies [21]. The key reducing agents responsible for converting zinc salt into ZnO-NPs are the proteins and amino acids present in the CFF of *P. chrysogenum* [23]. The observed color change during nanoparticle synthesis is attributed to the excitation of surface plasmon resonance (SPR) in the metal particles, which was confirmed through UV-visible spectroscopy. Since the position and shape of the SPR peak are strongly influenced by particle size, morphology, and the surrounding medium, UV-Vis analysis serves as a valuable tool for characterizing metal nanoparticles. In the present study, the SPR peak for ZnO-NPs synthesized using *Penicillium chrysogenum* cell-free filtrate (CFF) and $Zn(NO_3)_2 \cdot 6H_2O$ appeared at 430 nm, as shown in Figure 1A., confirming the formation of ZnO nanoparticles. These results are consistent with previous findings. Mohamed et al. [21], reported a UV–Vis absorption peak at 380 nm for ZnO-NPs synthesized using *P. chrysogenum* MF318506, while Sumanth et

al.[36] observed a maximum absorption at 370 nm when employing *Xylaria acuta* filtrate and zinc nitrate as precursors. Similarly, Shakib et al. [37], verified the formation of OM-ZnO NPs through UV-Vis spectroscopy, which showed a characteristic SPR peak at 368.8 nm. The slight red shift in the current study's SPR peak (430 nm) compared to previous reports may be attributed to variations in nanoparticle size, agglomeration, or differences in the composition of fungal metabolites acting as reducing and stabilizing agents.

Dynamic light scattering (DLS) analysis revealed a ZnO-NP size of 55.7 nm and a polydispersity index (PDI) of 0.47 as shown in Figure 1B. A previous study showed particle size distribution ranged from approximately 20 to 105 nm, with the highest frequency between 30 and 50 nm and an average size of 52 nm. The DLS spectrum further supported the presence of small-sized nanoparticles, correlating with the UV–Vis spectral peak at 370 nm [36].

The zeta potential of the biosynthesized ZnO nanoparticles was measured to assess their surface charge and colloidal stability. As shown in Figure 1C, the ZnO-NPs exhibited a zeta potential of –10.6 mV with a standard deviation of 3.64 mV, indicating a moderately stable colloidal system. The single, narrow peak in the zeta potential distribution suggests uniform surface charge and good particle dispersion without significant aggregation. Although nanoparticles with zeta potential values greater than ±30 mV are generally considered highly stable due to strong electrostatic repulsion, moderate stability (-10 to -30 mV) is often observed in biologically synthesized nanoparticles, as biomolecules (e.g., proteins, phenolics, and polysaccharides) serve as natural capping agents that reduce surface charge while providing steric stabilization. These findings are consistent with earlier studies reporting similar zeta potential values for myco-synthesized ZnO-NPs, such as -11.8 mV Mohamed et al. [21] and -13.2 mV according to Shakib et al., [37], suggesting that the nanoparticles possess sufficient stability for biomedical and biotechnological applications.

The diffractogram showed characteristic peaks at 2θ values of 29.5°, 34.46°, 38.26°, 43.5°, 47.5°, 49.54°, and 65°, corresponding to the (211), (202), (110), (114), (412), and (112) planes, respectively as shown in Figure 1D. Additional peaks at 2θ values of 31.72° (100), 34.47° (002), 36.25° (101), 47.71° (102), 56.59° (110), 62.98° (103), and 67.78° (112) confirmed the hexagonal phase of ZnO crystals [38]. Sumanth et al. [36] reported similar peaks corresponding to planes 100, 002, 101, 102, 110, 200, 103, 112, and 201, with 2θ values of 31.36°, 34.21°, 36.13°, 47.39°, 56.49°, 62.81°, 66.23°, 68.05°, and 69.16°. Using Scherrer's equation on the primary XRD peaks, the average crystallite size of the ZnO-NPs was estimated to be approximately 45 nm. The nanoscale nature of the particles was further supported by the broadening of the diffraction peaks [39]. Although the XRD pattern of the biosynthesized ZnO-NPs does not exhibit sharp and well-defined diffraction peaks typically observed for highly crystalline materials, the broad peaks observed correspond to the characteristic diffraction planes of ZnO (JCPDS Card No. 36-1451), confirming the formation of ZnO with a nanoscale crystallite size. The slight broadening and reduced intensity of the peaks may be attributed to the presence of organic capping agents derived from the *Penicillium chrysogenum* filtrate, which partially coat the nanoparticle surfaces and lead to reduced crystallinity. Similar findings have been reported in other biologically synthesized ZnO-NPs [21, 36, 37].
High-resolution transmission electron microscopy (HR-TEM) analysis revealed that the ZnO nanoparticles (ZnO-NPs) exhibited morphologies ranging from spherical to slightly irregular shapes. The 200 nm scale bar confirmed that the particles were within the nanometer range, with estimated diameters of approximately 50–70 nm. The nanoparticles appeared aggregated or clustered rather than uniformly dispersed, as shown in Figure 1E. The selected area electron diffraction (SAED) pattern, obtained from TEM, was employed to evaluate the crystalline structure of the ZnO-NPs. The presence of bright, sharp, and well-defined diffraction spots indicated that the ZnO-NPs possessed a crystalline nature. Additionally, the faint concentric rings observed in the SAED pattern suggested that the crystalline domains were randomly oriented or polycrystalline. The 5.00 $nm^{-1}$ scale bar corresponded to reciprocal lattice spacings, as illustrated in Figure 1F. Hexagonal and rod-shaped ZnO-NPs were also observed under 500 nm magnification, with average diameters ranging from 40 to 55 nm, consistent with previous reports [37]. Similarly, Abdelrahman *et al.* [22] characterized biosynthesized ZnO-NPs derived from *Aspergillus* sp. SA17 using both TEM and SEM, revealing spherical crystals ranging from 3 to 20 nm (average 7.2 nm) formed by the aggregation of smaller particles measuring 2–30 nm (average 28.9 nm). SEM micrographs further demonstrated agglomerated spherical ZnO-NPs with diameters between 13 and 55 nm (average 30 nm), supporting the observed diversity in nanoparticle morphology and size distribution.

### 3.2. Anti staphylococcal activity and MICs of ZnO-NPs

The anti-staphylococcal activity of biosynthesized ZnO-NPs was evaluated against methicillin-resistant

*Staphylococcus aureus* isolates using the agar well diffusion method. As presented in Figure 2 and Table 2, the biosynthesized ZnO-NPs exhibited potent antibacterial activity, producing inhibition zones of 29 ± 0.577 mm and 36 ± 0.882 mm. Given that antibacterial efficacy is often concentration-dependent, the MIC values of the ZnO-NPs were determined. The MIC results revealed effective inhibition of all MRSA isolates, with values ranging from 125 to 250 µg/mL, while the reference strain *S. aureus* ATCC 25923 displayed a MIC of 62.5 µg/mL (Table 3). Comparable findings have been reported by Asif et al. [40], who demonstrated the antimicrobial potency of ZnO-NPs against MRSA, with inhibition zones of 11.9 mm and 14 mm at concentrations of 150 µg/mL and 300 µg/mL, respectively. Similarly, Abdelraheem et al. [41] observed significant anti-MRSA activity, with MIC values ranging from 128 to 2048 µg/mL. These results collectively reinforce the growing body of evidence supporting the broad-spectrum antimicrobial potential of ZnO-NPs, particularly against multidrug-resistant strains such as MRSA.

Consequently, ZnO-NPs may represent promising alternatives or adjuncts to conventional antibiotics for the management of MRSA-associated infections [42]. The antibacterial mechanism of ZnO-NPs has been attributed primarily to the generation of reactive oxygen species (ROS), including hydroxyl radicals (•OH), hydrogen peroxide ($H_2O_2$), and superoxide anions ($O_2^{\bullet-}$), as reported by Jalal et al. [43]. In ZnO structures containing crystal defects, photoinduced electron–hole pairs ($e^-/h^+$) can form under UV or visible light irradiation. The photogenerated holes ($h^+$) oxidize water molecules to produce •OH radicals and protons ($H^+$), while the electrons ($e^-$) reduce dissolved oxygen to generate superoxide radicals. These radicals subsequently undergo reactions that yield hydroperoxyl radicals ($HO_2^{\bullet}$), hydroperoxide anions ($HO_2^-$), and ultimately hydrogen peroxide ($H_2O_2$). Among these species, $H_2O_2$ is particularly effective due to its membrane-permeable nature, allowing it to penetrate bacterial cells and disrupt intracellular components, leading to cell death [44]. In contrast, negatively charged species such as •OH and $O_2^{\bullet-}$ remain at the bacterial surface, causing localized oxidative damage without penetrating the cell membrane [4].

**Table 1.** Primers used in the PCR for the detection of virulence genes in MRSA

| Gene | Protein | Primer Sequence (5----------3′) | | Ref. |
|---|---|---|---|---|
| *16S rRNA* | | F | GTA GGT GGC AAG CGT TAT CC′ | [33] |
| | | R | CGCACATCAGCGTCAG | |
| *hla* | | F | TTAGCCGAAAAACATCATTTC | [2] |
| *hld* | Haemolysin | R | TTATTCCCGACGAAATTCCAA | |
| | | F | AAGAATTTTTATCTTAATTAAGGAAGGAGTG | |
| | | R | TTAGTGAATTTGTTCACTGTGTCGA | |
| *nuc* | Thermonuclease | F | GCGATTGATGGTGATACGGTT | [2] |
| | | R | AGCCAAGCCTTGACGAACTAAAGC | |
| *LukS/FPV* | Panton-Valentine Leucocidin | F | ATCATTAGGTAAAATGTCTGGACATGATCCA | [2] |
| | | R | GCATCAASTGTATTGGATAGCAAAAGC | |
| *spa* | *S. aureus* Protein A | F | CAAGCACCAAAAGAGGAA | [2] |
| | | R | CACCAGGTTTAACGACAT | |
| *coa* | Coagulase | F | CGAGACCAAGATTCAACAAG | [2] |
| | | R | AAAGAAAACCACTCACATCA | |
| *sea* | Enterotoxin A | F | GCAGGGAACAGCTTTAGGC | [2] |
| | | R | GTTCTGTAGAAGTATGAAACACG | |

**Table 2.** Antibacterial activity of the biosynthesized ZnO-NPs

| Bacterial strains | Mean of inhibition zone diameter mm (mean ± SD) | | | | |
|---|---|---|---|---|---|
| | 1 | 2 | 3 | 4 | 5 |
| MRSA1 | 0.0 | 0.0 | 0.0 | 0.0 | 15.021± 0.0 |
| MRSA2 | 0.0 | 0.0 | 0.0 | 9.03± 0.21 | 15.07± 0.51 |
| MRSA3 | 0.0 | 0.0 | 0.0 | 0.0 | 17.04± 0.20 |
| MRSA4 | 0.0 | 0.0 | 0.0 | 11.04± 0.20 | 12.01± 0.11 |
| MRSA5 | 0.0 | 0.0 | 0.0 | 13.05± 0.19 | 14.07± 0.49 |
| MRSA6 | 0.0 | 0.0 | 0.0 | 0.0 | 11.02± 0.70 |
| MRSA7 | 0.0 | 0.0 | 12.07± 0.20 | 0.0 | 27.024± 0.35 |
| SA-ATCC 25923 | 24.05± 0.21 | 14.02± 0.41 | 10.03± 0.70 | 25.07± 0.11 | 28.025± 0.31 |

1= Cefoxitin.2 = Ampicillin, 3 = Erythromycin, 4 = Gentamycin and 5 = ZnO-NPs

**Table 3.** MIC values of the biosynthesized ZnO-NPs

| No | Bacterial strains | MIC of ZnO-NPs (µg/ml) |
|---|---|---|
| 1 | MRSA1 | 125 |
| 2 | MRSA2 | 250 |
| 3 | MRSA3 | 125 |
| 4 | MRSA4 | 125 |
| 5 | MRSA5 | 125 |
| 6 | MRSA6 | 125 |
| 7 | MRSA7 | 125 |
| 8 | SA-ATCC 25923 | 62.5 |

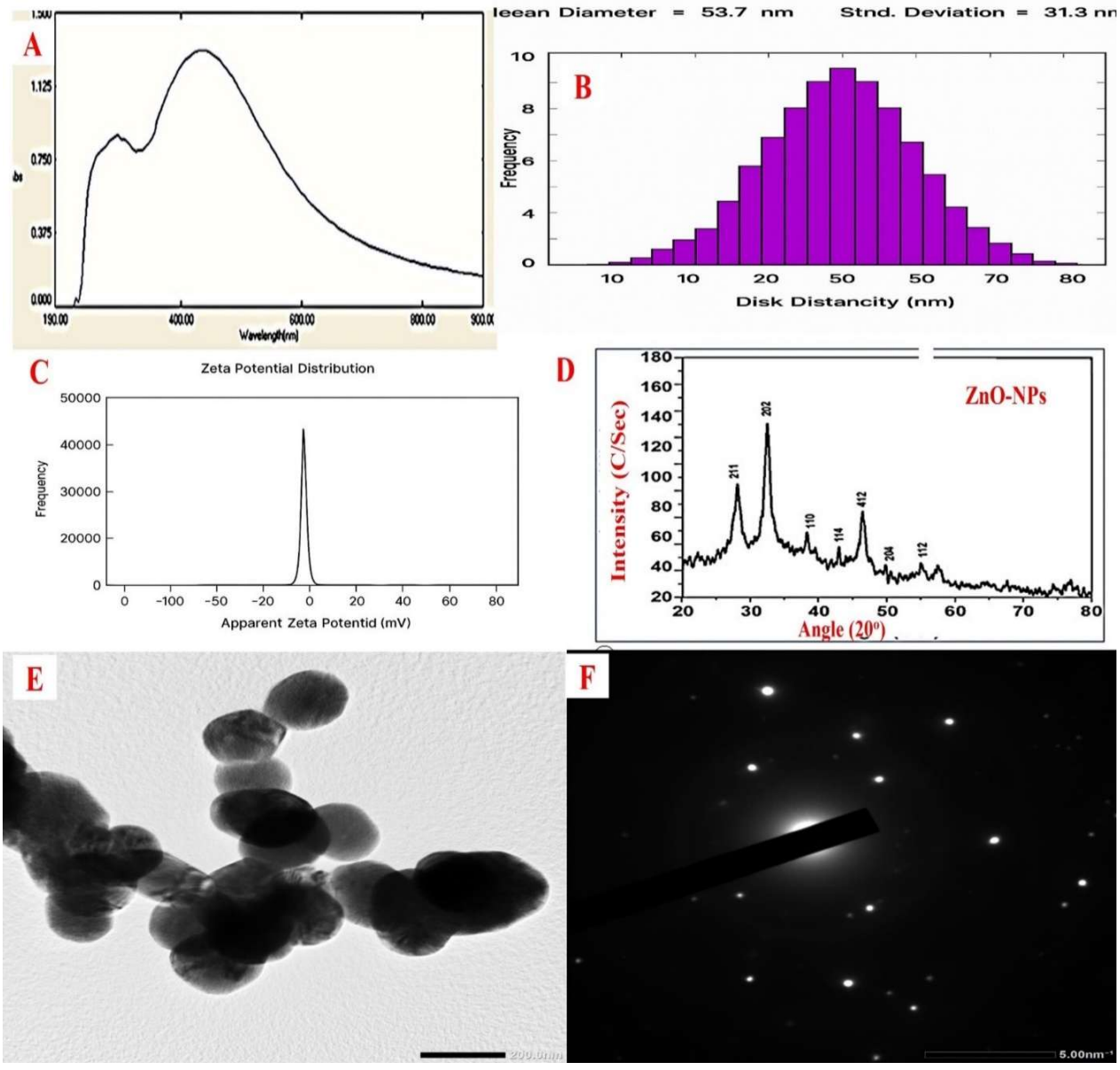


**Figure 1.** Characterization of biosynthesized ZnO nanoparticles: (A) UV–Visible spectral analysis confirming ZnO-NP formation; (B) dynamic light scattering (DLS) showing particle size distribution; (C) zeta potential analysis indicating surface charge stability; (D) X-ray diffraction (XRD) pattern confirming crystallinity; (E) high-resolution transmission electron microscopy (HR-TEM) micrograph depicting nanoparticle morphology; and (F) selected area electron diffraction (SAED) pattern illustrating the crystalline nature of the ZnO-NPs

10.57647/pibm-2025-17326

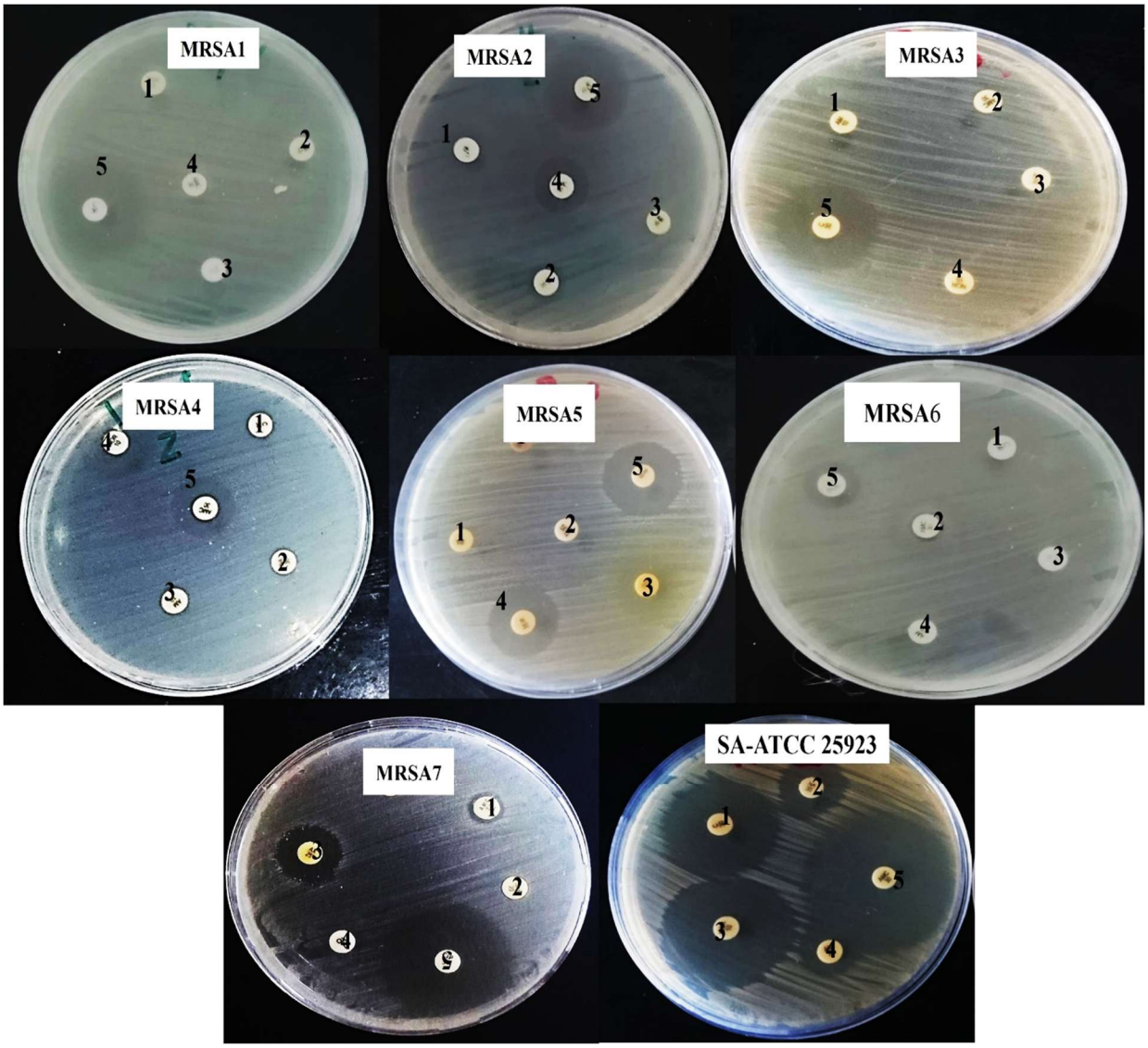


**Figure 3.** Antibacterial activity of the biosynthesized ZnO-NPs against MRSA isolates and standard strain ATCC 25923

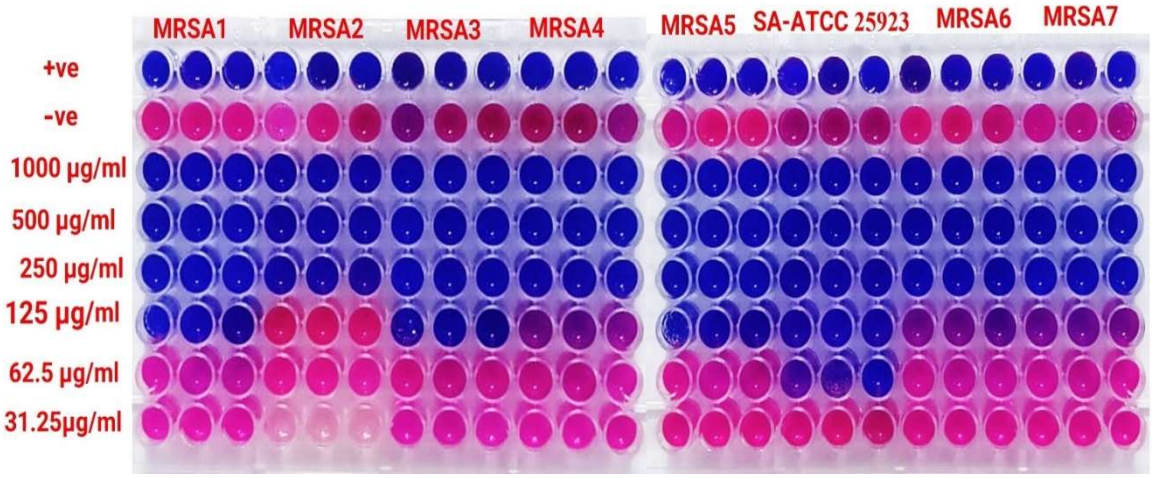


**Figure 2.** MIC of biosynthesized ZnO-NPs against MRSA isolates

### 3.3. Antibiofilm activity of biosynthesized ZnO-NPs

During the early stages of infection, planktonic bacterial cells actively attempt to adhere to surfaces or substrata to initiate colonization, ultimately leading to biofilm formation. Therefore, preventing this initial attachment step is crucial in the development of effective anti-biofilm strategies. In this study, the biosynthesized ZnO nanoparticles demonstrated notable anti-biofilm activity against MRSA isolates at various sub-inhibitory concentrations (⅛, ¼, and ½ MIC). The ½ MIC concentration showed the most significant biofilm inhibition, as illustrated in Figure 4. These findings are consistent with previous reports in which ZnO-NPs synthesized using *Penicillium chrysogenum* filtrate or plant extracts exhibited strong antibiofilm activity against a range of bacterial species [25, 45, 46]. Similarly, Banerjee et al. [47] reported the effective disruption of MRSA biofilms by ZnO-NPs. Biofilm formation is known to enhance bacterial resistance to antibiotics and impede the immune system's ability to eliminate the infection [48].

Given these challenges, it is imperative to develop alternative therapeutic agents that combine potent antimicrobial and anti-biofilm activities with minimal cytotoxicity. In this context, the ZnO-NPs synthesized in our study offer a promising solution. Compared to other metal-based nanoparticles, zinc oxide nanoparticles are generally regarded as less toxic and more biocompatible, making them suitable candidates for biomedical applications [47].

### 3.4. Effects of biosynthesized ZnO-NPs on expression virulence genes in MRSA isolates

*Staphylococcus aureus* harbors a wide array of virulence genes that contribute significantly to its pathogenicity. Therefore, targeting the downregulation of these genes may be a critical strategy in mitigating the bacterium's virulence. In this study, MRSA isolates treated with biosynthesized ZnO nanoparticles at half the MIC for an overnight period exhibited a significant reduction in the expression levels of several key virulence genes, including *nuc*, *lukS/F-PV*, *hla*, *hld*, *spa*, *coa*, and *sea*. The downregulation ranged from -2.0 to -4.6-fold (***P < 0. 0001) compared to the untreated control isolates, as shown in Figure 5.

These findings suggest that ZnO-NPs actively contribute to the suppression of virulence gene expression. Supporting this, a study by Shawky et al. [49] demonstrated that metal nanoparticles could downregulate virulence-associated genes in *Pseudomonas aeruginosa*. Similarly, Fareid et al. [1] reported that nanoparticles significantly reduced the expression of *icaA* and *icaD*, genes involved in biofilm formation, by -1.9 to -2.2 and -2.4 to -2.8-fold, respectively.

### 3.5. Antioxidant activity of ZnO-NPs

Nanoparticles have garnered significant attention due to their potential antioxidant properties, which play a crucial role in reducing oxidative stress and mitigating associated diseases. These nanoscale materials such as metal oxides and polymeric nanoparticles are capable of scavenging free radicals, thereby enhancing cellular defense mechanisms [50]. In the present study, the antioxidant potential of biosynthesized ZnO-NPs was evaluated using DPPH and ABTS assays to determine their free radical scavenging capacity. The DPPH analysis revealed that biosynthesized ZnO-NPs exhibited antioxidant activity with an $IC_{50}$ value of 205 µg/mL, in contrast to 8.9 µg/mL for ascorbic acid. Similarly, the ABTS assay yielded $IC_{50}$ values of 315 µg/mL for ZnO-NPs and 7.61 µg/mL for ascorbic acid, as shown in Figures 6A and 6B.

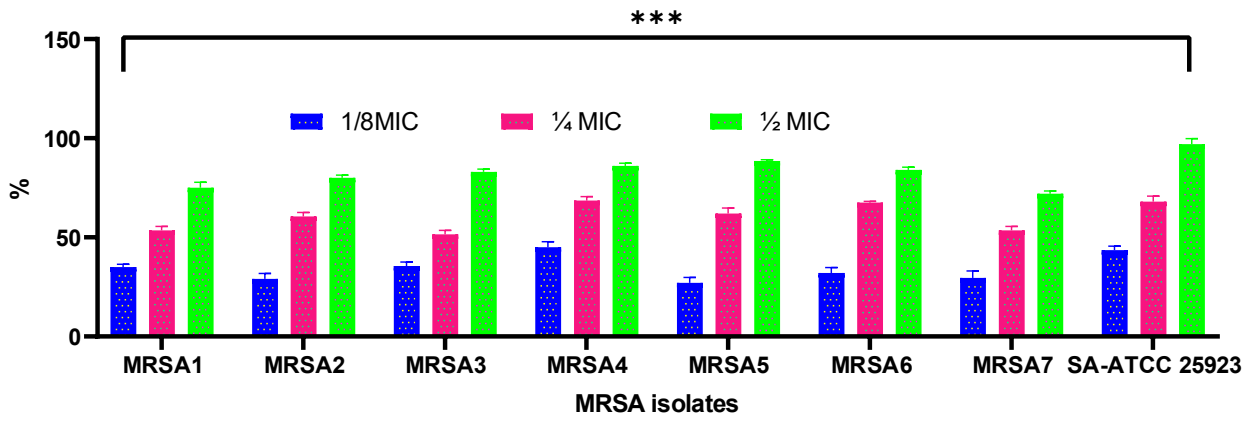


**Figure 4.** Antibiofilm activity of biosynthesized ZnO-NPs against MRSA isolates (*** $p \leq 0.001$).

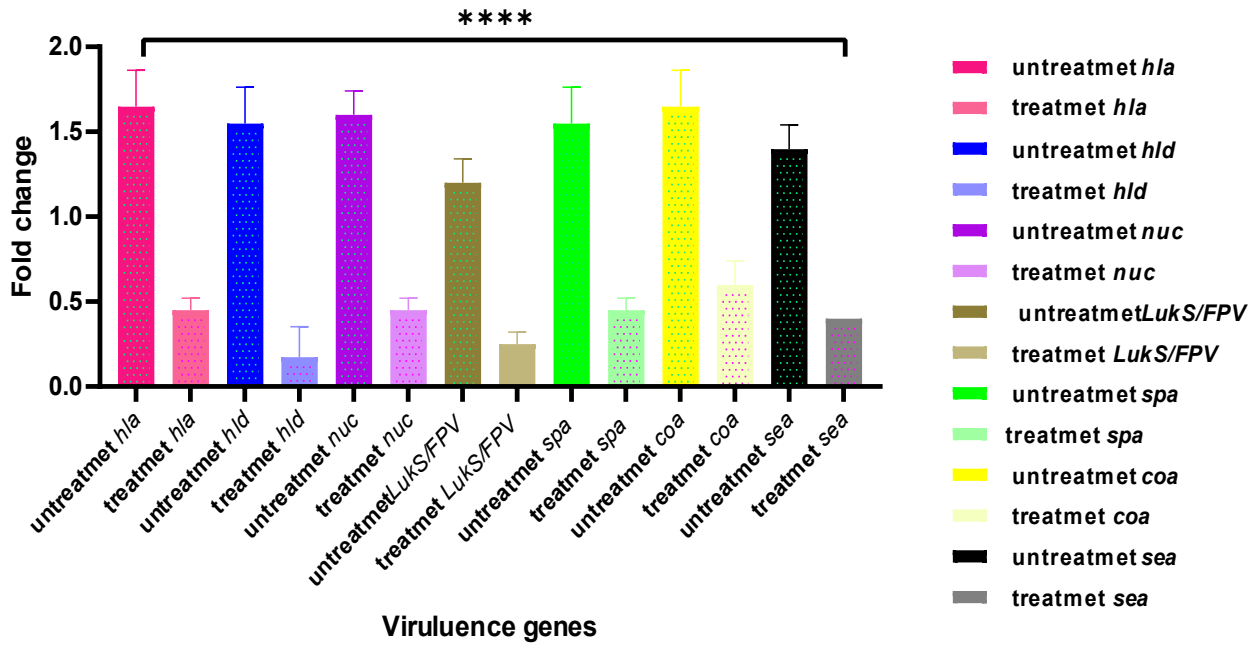


**Figure 5.** qRT-PCR expression of toxigenic genes (Nuc, LukS/FPV, hla, hld, spa, coa, and sea) in MRSA treated with ½ methanolic extract of ZnO-NPs and untreated (**** $p \leq 0.0001$)

These results indicate that, while ZnO-NPs possess measurable antioxidant activity, they are significantly less effective than ascorbic acid in scavenging free radicals.The DPPH assay, widely used for evaluating antioxidant activity, is particularly valued for its sensitivity in detecting active compounds even at low concentrations [51]. Our findings are consistent with a previous report by Elkady et al. [50], which demonstrated that ZnO-NPs biosynthesized using a *Mucor racemosus* filtrate exhibit notable antioxidant potential. The antioxidant activity of ZnO-NPs is primarily attributed to their ability to scavenge reactive oxygen species (ROS) and modulate oxidative stress-related pathways. These nanoparticles can neutralize free radicals through mechanisms involving electron transfer and radical quenching [52]. Additionally, ZnO-NPs may enhance the activity of key antioxidant enzymes such as superoxide dismutase (SOD) and catalase, which are critical for protecting cells from oxidative damage. The gradual release of $Zn^{2+}$ ions also contribute to the protective effects of ZnO-NPs by influencing cellular redox balance and upregulating the expression of antioxidant defense systems. These properties suggest that ZnO-NPs may hold promise as therapeutic agents for managing oxidative stress-related conditions, including neurodegenerative diseases, cardiovascular disorders, and inflammatory conditions. However, further studies are necessary to optimize their stability, bioavailability, and safe dosage for biomedical applications [53].

### 3.6. Anticancer activity of biosynthesized ZnO-NPs

Zinc oxide nanoparticles are considered among the most effective metal oxide nanoparticles used in cancer therapy due to their excellent biocompatibility, low toxicity, and ability to selectively target and destroy cancer cells by generating reactive oxygen species (ROS), which trigger apoptosis. In this study, the anticancer activity of biosynthesized ZnO-NPs was evaluated against HepG2 and MCF-7 cell lines at various concentrations compared to untreated control cells. The results demonstrated significant anticancer effects, with $IC_{50}$ values of 13.74 ± 0.02 µg/mL for HepG2 and 19.12 ± 0.51 µg/mL for MCF-7, as shown in Figure 7. Several previous studies have also reported the anticancer potential of biosynthesized ZnO-NPs [14, 46,50]. ZnO-NPs act as promising candidates for nanoparticle-based drug delivery systems in cancer chemotherapy, with the ability to selectively target tumor tissues, thereby providing a potential alternative to conventional treatments [42]. The anticancer properties of ZnO-NPs are primarily attributed to their ability to generate ROS and induce apoptosis. It has been widely documented that cancer cells exhibit significantly elevated ROS levels compared to normal cells following ZnO-NP treatment. Due to their high metabolic rates and rapid proliferation, cancer cells typically maintain increased levels of ROS and associated signaling molecules compared to normal cells [54-55]. Another advantageous feature of ZnO-NPs in anticancer applications is their electrostatic behavior. ZnO-NPs display unique surface charge characteristics due to the presence of neutral hydroxyl groups chemisorbed on their surface.

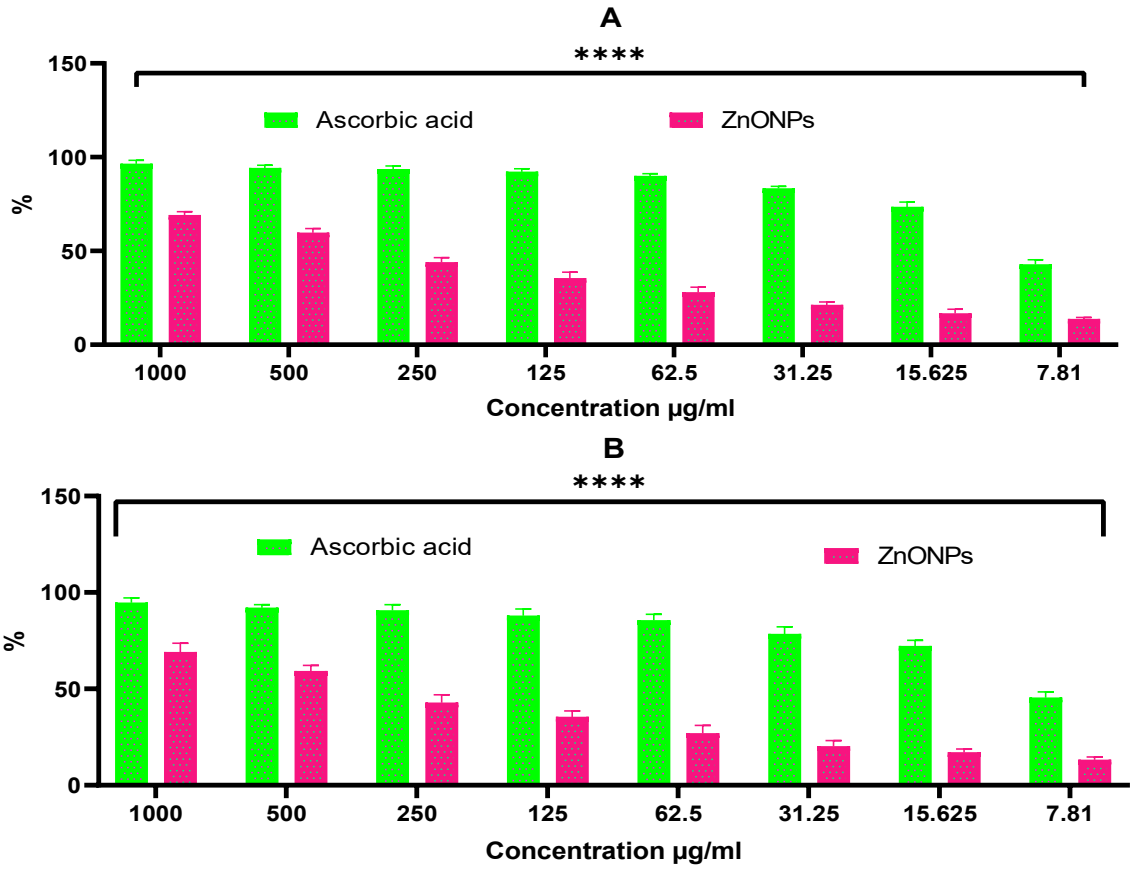


**Figure 6.** Antioxidant activity of biosynthesized ZnO-NPs, (A) DPPH and (B) ABTS (**** P <0.0001).

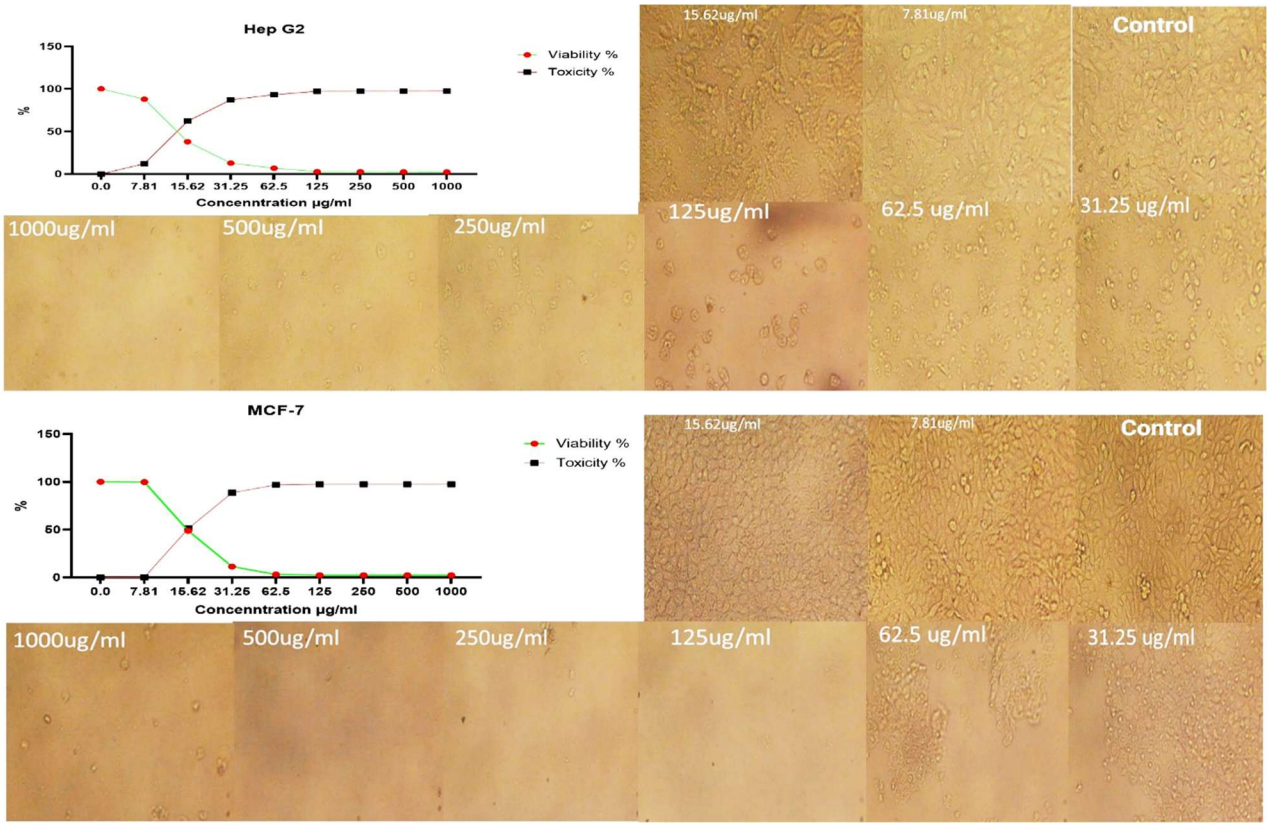


**Figure 7.** Anticancer activity of biosynthesized ZnO-NPs against HepG2 and MCf-7 cell lines

In aqueous media at high pH, the expulsion of protons ($H^+$) results in a negatively charged surface with partially bonded oxygen atoms ($ZnO^-$). In contrast, at lower pH levels, protons from the surrounding medium are adsorbed onto the surface, creating a positively charged surface ($ZnOH_2^+$). The isoelectric point of ZnO-NPs typically ranges from 9 to 10, meaning they possess a significant positive surface charge under physiological conditions [57,58]. Conversely, cancer cells display a high concentration of anionic phospholipids (particularly phosphatidylserine) on their outer membranes and have a substantially negative membrane potential. This contrast enhances the selective interaction of positively charged ZnO-NPs with cancer cells [59,60].

## 4. Conclusion

This study successfully demonstrated a green, sustainable, and efficient approach for the biosynthesis of ZnO-NPs using the cell-free filtrate of *Penicillium chrysogenum*. Comprehensive characterization confirmed the formation of well-defined, nanosized particles with distinct morphologies. The biosynthesized ZnO-NPs exhibited potent antibacterial activity against multidrug-resistant bacteria, particularly methicillin-resistant *Staphylococcus aureus*, through significant inhibition of biofilm formation and downregulation of key virulence-associated genes. In addition, they showed strong antioxidant capacity and pronounced anticancer effects against MCF-7 (breast) and HepG2 (liver) cell lines, highlighting their potential in biomedical and therapeutic applications. The novelty of this research lies in the first-time utilization of *P. chrysogenum* filtrate as a biological template for ZnO-NP synthesis, establishing an eco-friendly alternative to conventional chemical routes. These findings position the biosynthesized ZnO-NPs as promising multifunctional nanomaterials with antibacterial, anti-virulence, antioxidant, and anticancer properties. Nevertheless, further studies are warranted to expand their evaluation against a wider range of pathogens and to conduct in vivo investigations to determine their biocompatibility, pharmacokinetic behavior, and therapeutic efficacy. Such efforts will be crucial for translating these biosynthesized ZnO-NPs into viable, eco-friendly nanotherapeutic candidates for clinical and industrial applications.

**Funding**
This research has been funded by Scientific Research Deanship at University of Ha'il - Saudi Arabia through project number: RG-24 070.

**Acknowledgment**
All authors thank the Scientific Research Deanship at University of Ha'il for their grant through a project number: RG-24 070

**Ethical approval**
All studies have been reviewed and approved by the Research Ethics Committee (REC) at University of Ha'il - Saudi Arabia (Approval No., H-2024-519).

**Clinical trial number:**
not applicable.'

**AI tools**
No generative AI tools were used in the preparation of this manuscript

**Authors Contribution**
All authors have contributed equally to prepare the paper.

**Availability of data and materials**
All data generated or analyzed during this study are included in this published article.

**Conflict of interests**
The authors declare no conflicts of interest.

## References

[1] Fareid, M.A.; El-Sherbiny, G.M.; Askar, A.A.; Abdelaziz, A.M.; Hegazy, A.M.; Ab Aziz, R.; Hamada, F.A. Impeding Biofilm-Forming Mediated Methicillin-Resistant *Staphylococcus aureus* and Virulence Genes Using a Biosynthesized Silver Nanoparticles–Antibiotic Combination. *Biomolecules* 2025, *15*, 266.

[2] Wilson TK, Zishiri OT, El Zowalaty ME. Molecular detection of multidrug and methicillin resistance in *Staphylococcus aureus* isolated from wild pigeons (*Columba livia*) in South Africa. One Health. 2024 Jan 1; 18:100671.

[3] Bastidas CA, Villacrés-Granda I, Navarrete D, Monsalve M, Coral-Almeida M, Cifuentes SG. Antibiotic susceptibility profile and prevalence of *mec*A and *lukS-PV/lukF-PV* genes in *Staphylococcus aureus* isolated from nasal and pharyngeal sources of medical students in Ecuador. Infect Drug Resist. 2019 Aug 16; 12:2553-2560.

[4] Kalaba, M.H., El-Sherbiny, G.M., Ewais, E.A. *et al.* green synthesis of zinc oxide nanoparticles (ZnO-NPs) by *Streptomyces baarnensis* and its active metabolite (Ka): a promising combination against multidrug-resistant ESKAPE pathogens and cytotoxicity. *BMC Microbiol* 24, 254 (2024).

[5] Shawky, M., Kalaba, M.H. & El-Sherbiny, G.M. Combined impact of biosynthesized selenium nanoparticles and imipenem against carbapenem-resistant *Pseudomonas aeruginosa* and their associated virulence factors. *BMC Microbiol* 25, 235 (2025).

[6] El-Sherbiny, G. M., Kalaba, M. H., Sharaf, M. H., Moghannem, S. A., Radwan, A. A., Askar, A. A., … Abushiba, M. A. (2022). Biogenic synthesis of CuO-NPs as nanotherapeutics approaches to overcome multidrug-resistant *Staphylococcus aureus* (MDRSA). *Artificial Cells, Nanomedicine, and Biotechnology*, *50*(1), 260–274.

[7] Rao, M.P.N. (2023) Fungal synthesis of zinc oxide nanoparticles and its applications in biomedical, environmental, and agri-food sectors. In: Fungal Cell Factories for Sustainable Nanomaterials Productions and Agricultural Applications, pp. 115–130. Elsevie.

[8] Nehru, L., Kandasamy, G. D., Sekar, V., Alshehri, M. A., Panneerselvam, C., Alasmari, A., & Kathirvel, P. (2023). Green synthesis of ZnO-NPs using endophytic fungal extract of *Xylaria arbuscula* from *Blumea axillaris* and its biological applications. *Artificial Cells, Nanomedicine, and Biotechnology*, *51*(1), 318–333. DOI: https://doi.org/10.1080/21691401.2023.2232654

[9] Purushotham D, Mavinakere Ramesh A, Shetty Thimmappa D, Kalegowda N, Hittanahallikoppal Gajendramurthy G, Kollur SP, Mahadevamurthy M. Green Synthesis of Zinc Oxide Nanoparticles Using Aqueous Extract of *Pavonia zeylanica* to Mediate Photocatalytic Degradation of Methylene Blue: Studies on Reaction Kinetics, Reusability and Mineralization. *International Journal of Molecular Sciences*. 2025; 26(10):4739.

[10] Mishra P, Ahmad A, Al-Keridis LA, et al. Doxorubicin-conjugated zinc oxide nanoparticles, biogenically synthesized using a fungus *Aspergillus niger*, exhibit high therapeutic efficacy against lung cancer cells. Molecules. 2022;27(8):2590. DOI: https://doi.org/10.3390/molecules27082590

[11] Kaur T, Bala M, Kumar G, et al. Biosynthesis of zinc oxide nanoparticles via endophyte Trichoderma viride and evaluation of their antimicrobial and antioxidant properties. Arch Microbiol. 2022;204(10):620. DOI: https://doi.org/10.1007/s00203-022-03218-9

[12] Sumanth B, Lakshmeesha TR, Ansari MA, et al. Mycogenic synthesis of extracellular zinc oxide nanoparticles from Xylaria acuta and its nanoantibiotic potential. IJN. 2020; ume 15:8519–8536.) DOI: https://doi.org/10.2147/IJN.S271743

[13] Abdelhakim HK, El-Sayed ER, Rashidi FB. Biosynthesis of zinc oxide nanoparticles with antimicrobial, anticancer, antioxidant and photocatalytic activities by the endophytic alternaria tenuissima. J Appl Microbiol. 2020;128(6):1634–1646.

[14] Kadam VV, Ettiyappan JP, Balakrishnan RM. Mechanistic insight into the endophytic fungus mediated synthesis of protein capped ZnO nanoparticles. Mat Sci Eng b. 2019; 243:214–221. DOI: https://doi.org/10.1016/j.mseb.2019.04.017

[15] El-Sayed ESR, Mousa SA, Abdou DA, et al. Exploiting the exceptional biosynthetic potency of the endophytic Aspergillus terreus in enhancing production of Co3O4, CuO, $Fe_3O_4$, NiO, and ZnO nanoparticles using bioprocess optimization and gamma irradiation. Saudi J Biol Sci. 2022;29(4):2463–2474.

[16] Cheraghipour K, Khudair Khalaf A, Moradpour K, Zivdari M, Beiranvand M, Shakib P, Mahmoudvand H, Marzban A. Synthesis, characterization, and antiparasitic effects of zinc oxide nanoparticles-eugenol nanosuspension against *Toxoplasma gondii* infection. Heliyon. 2023 Aug 19;9(8):e19295. DOI: https://doi.org/10.1016/j.heliyon. 2023.e19295. PMID: 37654466; PMCID: PMC10465954

[17] Gilavand F, Saki R, Mirzaei S Z, Lashgarian H E, Karkhane A, Marzban A. Green Synthesis of Zinc Nanoparticles Using Aqueous Extract of Magnoliae officinalis and Assessment of its Bioactivity Potentials. Biointerface Research in Applied Chemistry. 11(1), 2021, 7765 - 7774 DOI: https://doi.org/10.33263/BRIAC111.77657774

[18] Karkhane M, Lashgarian HE, Mirzaei SZ, Ghaffarizadeh A, Cherghipour K, Sepahvand A, Marzban A. Antifungal, antioxidant and photocatalytic activities of zinc nanoparticles synthesized by *Sargassum vulgare* extract. Biocatalysis and Agricultural Biotechnology 29, 2020, 101791. DOI: https://doi.org/10.1016/j.bcab.2020.101791Get rights and content

[19] Cheraghipour K, Azarhazine M, Zivdari M, Beiranvand M, Shakib P, Rashidipour M, Mardanshah O, Mohaghegh MA, Marzban A. Evaluation of scolicidal potential of salicylate coated zinc nanoparticles against Echinococcus granulosus protoscoleces. Exp Parasitol. 2023 Mar;246:108456. DOI: https://doi.org/10.1016/j.exppara.2022.108456. Epub 2023 Jan 5. PMID: 36610471

[20] Kumar RV, Vinoth S, Baskar V, et al. Synthesis of zinc oxide nanoparticles mediated by Dictyota dichotoma endophytic fungi and its photocatalytic degradation of fast green dye and antibacterial applications. S Afr J Bot. 2022; 151:337–344.

[21] Mohamed, A.A., Abu-Elghait, M., Ahmed, N.E. *et al.* Eco-friendly Mycogenic Synthesis of ZnO and CuO Nanoparticles for In Vitro Antibacterial, Antibiofilm, and Antifungal Applications. *Biol Trace Elem Res* 199, 2788–2799 (2021).

[22] Abdelrahman SESAH, El Hawary S, Mohsen E, El Raey MA, Selim HMRM, Hamdan AME, Ghareeb MA, Hamed AA. Bio-fabricated zinc oxide nanoparticles mediated by endophytic fungus *Aspergillus* sp. SA17 with antimicrobial and anticancer activities: *in vitro* supported by *in silico* studies. Front Microbiol. 2024 May 13; 15:1366614.

[23] El-Sherebiny GM, Ali AR, Ali DM, Ahamed S, El-Hawary AS, Askar AA. Bioengineering of Zinc Oxide nanoparticles as therapeutics for Immunomodulatory and Antimicrobial activities. Egypt J Chem Vol. 2022; 65:1473–86. SI:13.

[24] Morowvat MH, Kazemi K, Jaberi MA, Amini A, Gholami A. Biosynthesis and Antimicrobial Evaluation of Zinc Oxide Nanoparticles Using *Chlorella vulgaris* Biomass against Multidrug-Resistant Pathogens. Materials (Basel). 2023 Jan 15;16(2):842. doi: 10.3390/ma16020842. PMID: 36676578; PMCID: PMC9863921.

[25] Vinotha V, Yazhiniprabha M, Jeyavani J, Vaseeharan B. Synthesis and characterization of cry protein coated zinc oxide nanocomposites and its assessment against bacterial biofilm and mosquito vectors. Int J Biol Macromol. 2022 May 31; 208:935-947. DOI: https://doi.org/10.1016/j.ijbiomac.2022.03.165. Epub 2022 Mar 30. PMID: 35364199

[26] Azizi-Lalabadi M, Ehsani A, Divband B and Alizadeh-Sani M: Antimicrobial activity of titanium dioxide and zinc oxide nanoparticles supported in 4A zeolite and evaluation the morphological characteristic. Sci Rep. 9(17439)2019.

[27] Banerjee S, Vishakha K, Das S, Dutta M, Mukherjee D, Mondal J, Mondal S and Ganguli A: Antibacterial, anti-biofilm activity

and mechanism of action of pancreatin doped zinc oxide nanoparticles against methicillin resistant *Staphylococcus aureus*. Colloids Surf B Biointerfaces. 190(110921)2020

[28] Zare, E., Pourseyedi, S., Khatami, M. and Darezereshki, E., 2017. Simple biosynthesis of zinc oxide nanoparticles using nature's source, and it's in vitro bioactivity. Journal of Molecular Structure, 1146, pp.96-103

[29] El-Sherbiny, G.M.; Kalaba, M.H.; Foda, A.M.; ME, S.; Youssef, A.S.E.; AElsehemy, I.; Farghal, E.E.; El-Fakharany, E.M. Nanoemulsion of cinnamon oil to combat colistin-resistant Klebsiella pneumoniae and cancer cells. *Microb. Pathog.* 2024, *192*, 106705.

[30] Abdel-Fatah, S.S.; El-Sherbiny, G.M.; khalaf, M. Boosting the Anticancer activity of *aspergillus flavus* endophyte of Jojoba Taxol via conjugation with gold nanoparticles mediated by γ-Irradiation. *Appl. Biochem. Biotechnol.* 2022, *194*, 3558–3581

[31] Mkize N, Zishiri OT, Mukaratirwa S. Genetic characterisation of antimicrobial resistance and virulence genes in *Staphylococcus aureus* isolated from commercial broiler chickens in the Durban metropolitan area, South Africa. J S Afr Vet Assoc. 2017 May 4;88(0):e1-e7

[32] Monday SR, Bohach GA. Use of multiplex PCR to detect classical and newly described pyrogenic toxin genes in staphylococcal isolates. J Clin Microbiol. 1999;37(10):3411–4.

[33] Higuera-Llantén S, Vásquez-Ponce F, Barrientos-Espinoza B, Mardones FO, Marshall SH, Olivares-Pacheco J. Extended antibiotic treatment in salmon farms select multi-resistant gut bacteria with a high prevalence of antibiotic resistance genes. PLoS ONE. 2018;13(9): e0203641.

[34] El-Sherbiny, G.M.; Gazelly, A.M.; Sharaf, M.H.; Moghannemm, S.A.; Shehata, M.; Ismail, M.K.A.; El-Hawary, A.S. Exploitation of the antibacterial, antibiofilm and antioxidant activities of *Salvadora persica* (Miswak) extract. *J. Bioresour. Bioprod.* 2022, *8*, 59–65

[35] El-Sherbiny, G.M., Alluqmani, A.J., Elsehemy, I.A. *et al.* Antibacterial, antioxidant, cytotoxicity, and phytochemical screening of *Moringa oleifera* leaves. *Sci Rep* 14, 30485 (2024).
DOI: https://doi.org/10.1038/s41598-024-80700-y

[36] Sumanth B, Lakshmeesha TR, Ansari MA, Alzohairy MA, Udayashankar AC, Shobha B, Niranjana SR, Srinivas C, Almatroudi A. Mycogenic Synthesis of Extracellular Zinc Oxide Nanoparticles from *Xylaria acuta* and Its Nanoantibiotic Potential. Int J Nanomedicine. 2020 Nov 2; 15:8519-8536.

[37] Shakib P, Mirzaei SZ, Lashgarian HE, Saki R, Goudarzi G, Alsallameh S, Marzban A, Cheraghipour K. Preparation of Zinc Oxide Nanoparticles Assisted by Okra Mucilage and Evaluation of its Biological Activities. Curr Drug Discov Technol. 2023;20(2):e011222211472.
DOI: https://doi.org/10.2174/1570163820666221201090006. PMID: 36464868

[38] Mohamed AA, Fouda A, Abdel-Rahman MA, Hassan SE-D, El-Gamal MS, Salem SS, Shaheen TI (2019) Fungal strain impacts the shape, bioactivity and multifunctional properties of green synthesized zinc oxide nanoparticles. Biocatal Agric Biotechnol 19:101103

[39] Lepot N, Van Bael MK, Van den Rul H, et al. Synthesis of ZnO nanorods from aqueous solution. *Mater Lett*. 2007;61(13):2624–2627.
DOI: https://doi.org/10.1016/j.matlet.2006.10.025

[40] Asif M, Chaudhry AS, Ashar A, Bin Rashid H Saleem, Bin Aslam H, Abdul Aziz MH Zinc oxide nanoparticles accelerate the healing of methicillin-resistant *Staphylococcus aureus* (MRSA)-infected wounds in rabbits. Asian Pacific Journal of Tropical Biomedicine 2023; 13(11): 488-496

[41] Abdelraheem WM, Khairy RMM, Zaki AI, Zaki SH. Effect of ZnO nanoparticles on methicillin, vancomycin, linezolid resistance and biofilm formation in Staphylococcus aureus isolates. Ann Clin Microbiol Antimicrob. 2021 Aug 21;20(1):54.
DOI: https://doi.org/10.1186/s12941-021-00459-2. PMID: 34419054; PMCID: PMC8379777

[42] Mishra PK, Mishra H, Ekielski A, Talegaonkar S, Vaidya B. Zinc oxide nanoparticles: a promising nanomaterial for biomedical applications. Drug Discov Today. 2017 Dec;22(12):1825-1834.

[43] Jalal R, Goharshadi EK, Abareshi M, Moosavi M, Yousefi A, Nancarrow P. ZnO nanofluids: green synthesis, characterization, and antibacterial activity. Materials Chemistry and Physics. 121, (1–2, 15) 2010, 198-201.

[44] Shende, S., Ingle, A. P., Gade, A. and Rai, M. (2015). Green synthesis of copper nanoparticles by Citrus medica Linn. (Idilimbu) juice and its antimicrobial activity. *World Journal of Microbiology and Biotechnology*, 31(6), 865-873

[45] Husain FM, Qais FA, Ahmad I, Hakeem MJ, Baig MH, Masood Khan J, Al-Shabib NA. Biosynthesized Zinc Oxide Nanoparticles Disrupt Established Biofilms of Pathogenic Bacteria. *Applied Sciences*. 2022; 12(2):710.
DOI: https://doi.org/10.3390/app12020710

[46] Almuhayawi MS, Alruhaili MH, Soliman MKY, Tarabulsi MK, Ashy RA, Saddiq AA, et al. (2024) Investigating the *in vitro* antibacterial, antibiofilm, antioxidant, anticancer and antiviral activities of zinc oxide nanoparticles biofabricated from *Cassia javanica*. PLoS ONE 19(10): e0310927.
DOI: https://doi.org/10.1371/journal.pone.0310927

[47] Banerjee S, Vishakha K, Das S, Dutta M, Mukherjee D, Mondal J, Mondal S, Ganguli A. Antibacterial, anti-biofilm activity and mechanism of action of pancreatin doped zinc oxide nanoparticles against methicillin resistant Staphylococcus aureus. Colloids Surf B Biointerfaces. 2020 Jun; 190:110921.
DOI: https://doi.org/10.1016/j.colsurfb.2020.110921. Epub 2020 Mar 4. PMID: 32172163

[48] Ricciardi BF, Muthukrishnan G, Masters E, Ninomiya M, Lee CC, Schwarz EM. Staphylococcus aureus Evasion of Host Immunity in the Setting of Prosthetic Joint Infection: Biofilm and Beyond. Curr Rev Musculoskelet Med. 2018 Sep;11(3):389-400. doi: 10.1007/s12178-018-9501-4.

[49] Shawky, M., Kalaba, M.H. & El-Sherbiny, G.M. Combined impact of biosynthesized selenium nanoparticles and imipenem against carbapenem-resistant *Pseudomonas aeruginosa* and their associated virulence factors. *BMC Microbiol* 25, 235 (2025).

DOI: https://doi.org/10.1186/s12866-025-03932-6

[50] Elkady, F.M., Badr, B.M., Saied, E. *et al.* Mycosynthesis of zinc oxide nanoparticles using *Mucor racemosus* with their antimicrobial, antibiofilm, anticancer and antioxidant activities. *Sci Rep* 15, 18772 (2025). DOI: https://doi.org/10.1038/s41598-025-03421-w

[51] El-Sayed, M. H., Alshammari, F. A., & Sharaf, M. H. (2023). Antagonistic potentiality of actinomycete-derived extract with anti-biofilm, antioxidant, and cytotoxic capabilities as a natural combating strategy for multidrug-resistant ESKAPE pathogens. Journal of Microbiology and Biotechnology, 33(1), 61.

[52] Dai, Y. et al. Reactive oxygen species-scavenging nanomaterials for the prevention and treatment of age-related diseases. *J. Nanobiotechnol.* 22 (1), 252. DOI: https://doi.org/10.1186/s12951-024-02501-9 (2024)

[53] Murali, M., Kalegowda, N., Gowtham, H. G. & Ansari, M. A. Plant-mediated zinc oxide nanoparticles: advances in the new millennium towards understanding their therapeutic role in biomedical applications. *Pharmaceutics* 13(10).

[54] Anjum S, Hashim M, Malik SA, et al. Recent advances in Zinc Oxide nanoparticles (ZnO NPs) for Cancer diagnosis, Target Drug Delivery, and treatment. Cancers. 2021;13(18):4570.

[55] Hanley C, Layne J, Punnoose A, et al. Preferential killing of cancer cells and activated human T cells using ZnO nanoparticles. Nanotechnology. 2008;19(29):295103.

[56] Dou Q, Fang X, Jiang S, Chee PL, Lee TC, Loh XJ. Multi-functional fluorescent carbon dots with antibacterial and gene delivery properties. RSC Adv. 2015;5(58):46817–22.

[57] F.Y. Qu, P.C. Morais The pH dependence of the surface charge density in oxide-based semiconductor nanoparticles immersed in aqueous solution IEEE Trans. Magn., 37 (2001), pp. 2654-2656

[58] Degen, M. Kosec Effect of pH and impurities on the surface charge of zinc oxide in aqueous solution. J. Eur. Ceram. Soc., 20 (2000), pp. 667-673

[59] M. Abercrombie, E.J. Ambrose The surface properties of cancer cells: a review. Cancer Res., 22 (1962), pp. 525-548

[60] S.D. Vallabhapurapu, *et al.* Variation in human cancer cell external phosphatidylserine is regulated by flippase activity and intracellular calcium Oncotarget, 6 (2015), pp. 34375-34388